AD-A092 568 NAVAL RESEARCH LAB WASHINGTON DC F/6 4/1

SCALE SIZES AND LIFETIMES OF F REGION PLASMA CLOUD STRIATIONS A--ETC(U)

NOV 80 B E MCDONALD, S L OSSAKOW, S T ZALESAK

UNCLASSIFIED NRL-MR-4383 NL

1 OF 1

AD A 092568

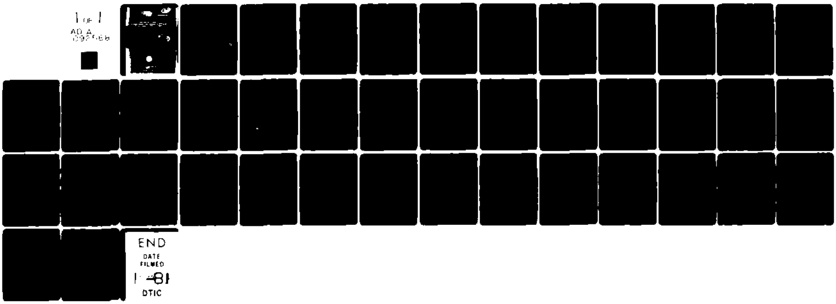

END

DATE FILMED

1-81

DTIC

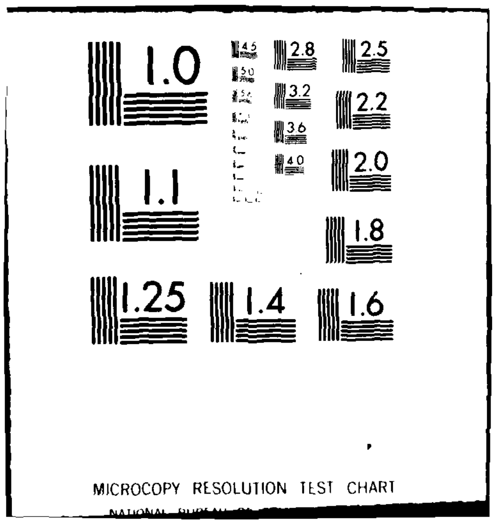
1.0
1.1
1.25
1.4
1.6
1.8
2.0
2.2
2.5
2.8
3.2
3.6
4.0
MICROCOPY RESOLUTION TEST CHART

AD A092568

(9) Memorandum rept.

SECURITY CLASSIFICATION OF THIS PAGE (When Data Entered)

REPORT DOCUMENTATION PAGE

READ INSTRUCTIONS BEFORE COMPLETING FORM

1. REPORT NUMBER (14) NRL-MR- NRL Memorandum Report 4383	2. GOVT ACCESSION NO. AD-A092	3. RECIPIENT'S CATALOG NUMBER 568
4. TITLE (and Subtitle) (6) SCALE SIZES AND LIFETIMES OF F REGION PLASMA CLOUD STRIATIONS AS DETERMINED BY THE CONDITION OF MARGINAL STABILITY.		5. TYPE OF REPORT & PERIOD COVERED Interim report on a continuing basis. 6. PERFORMING ORG. REPORT NUMBER
7. AUTHOR(s) (10) B. E. McDonald, S. L. Ossakow, S. T. Zalesak, and N. J. Zabusky*		8. CONTRACT OR GRANT NUMBER(s) (11) 17 Nov 80
9. PERFORMING ORGANIZATION NAME AND ADDRESS Naval Research Laboratory Washington, DC 20375 (12) 42		10. PROGRAM ELEMENT, PROJECT, TASK AREA & WORK UNIT NUMBERS 67-0889-0-0
11. CONTROLLING OFFICE NAME AND ADDRESS Defense Nuclear Agency Washington, DC 20305		12. REPORT DATE November 17, 1980 13. NUMBER OF PAGES 41
14. MONITORING AGENCY NAME & ADDRESS(if different from Controlling Office)		15. SECURITY CLASS. (of this report) UNCLASSIFIED 15a. DECLASSIFICATION/DOWNGRADING SCHEDULE

16. DISTRIBUTION STATEMENT (of this Report)

Approved for public release: distribution unlimited.

DTIC ELECTE DEC 4 1980 D

17. DISTRIBUTION STATEMENT (of the abstract entered in Block 20, if different from Report)

18. SUPPLEMENTARY NOTES

*Present address: University of Pittsburgh, Pittsburg, PA
This research was sponsored by the Defense Nuclear Agency under subtask (16) S99QAXHC041, work unit 21, and work unit title "Plasma Structure Evolution."

19. KEY WORDS (Continue on reverse side if necessary and identify by block number)

Plasma striations
Gradient drift
Bifurcation
Striation "freezing"
Scale sizes
Computer simulations

(17) C041

20. ABSTRACT (Continue on reverse side if necessary and identify by block number)

The two dimensional integrated Pedersen conductivity model for F region plasma cloud striation development may be cast in dimensionless form. The result implies that a structure's stability against bifurcation depends upon whether a diffusion parameter R exceeds a critical value. The critical R for striations is determined by high resolution computer simulation for conductivity ratios M from 2 to 30. Our results combined with electron diffusivity of order 1 m^2/sec agree with observed minimum scale sizes of 15 meters. For turbulent diffusivity of order

(Continues)

251950

20. Asbtract (continued)

square meter

100 m^2/sec, our results agree with frequent observations of kilometer-scale structures which "freeze up" and last for times of order 10^4 seconds. This lifetime is also predicted by our results.

10,000

CONTENTS

SCALE SIZES AND LIFETIMES OF F REGION PLASMA CLOUD STRIATIONS AS DETERMINED BY THE CONDITION OF MARGINAL STABILITY

1. Introduction

Phenomenologists have been pressed to account for certain features of late time barium cloud striations, despite the early time success and near universal acceptance of results from the $\underline{E} \times \underline{B}$ gradient drift instability theory [Linson and Workman, 1970; Perkins et al., 1973, Francis and Perkins, 1975]. We refer to the simultaneous occurrence of three phenomena as documented in the 1977 STRESS program: a) the generation of structure on scales as small as 15 meters [Baker and Ulwick, 1978];b) the apparent ubiquity of visible striations separated by distances approaching one kilometer; and c) the survival for hours (sometimes referred to as "freezing up") of this kilometer-scale structure as evidenced by propagation studies [Prettie et al., 1977]. If the gradient drift instability is at work producing small structure through a series of bifurcations, why do the kilometer scale structures persist? What parameters select out the kilometer scale size so often? (Observers have often noted that visible structuring seems to halt when scale sizes transverse to the neutral wind direction decrease to just under one kilometer [J. A. Fedder, W. Chestnut, private communication, 1980]. Past this point, there is a tendency for the striations to drift in unison as long as they can be seen.)

We support the gradient drift instability as the explanation for striation behavior. In fact, the emergence at late times of density power law spectra from numerical simulations [Scannapieco, et al. 1976] is in agreement with observation [Baker and Ulwick, 1978]. We feel, however, that attempts to explain the above mentioned three features have been hindered by approaching the problem from two opposite extremes: 1) application of analytic

Manuscript submitted September 29, 1980.

results from an idealized one dimensional slab model; and 2) brute force case-by-case numerical simulation beginning with an initially smooth plasma distribution, and proceeding toward a highly structured state. One is not surprised that some disagreement exists between an idealized linear result and the highly structured nonlinear environment. On the other extreme, global numerical simulation on present day computers must eventually be hindered by inadequate resolution. We feel, too, that the role of diffusion (both classical and turbulent) has not been sufficiently emphasized in determining late time structure. This is partly because present day computers cannot resolve both the global cloud scale and the diffusion scale due to storage and speed limitations. In order to fill in these gaps, we shall extract from the basic one level (F region) striation model a scaling law which allows individual structures to provide information concerning "bifurcation tendencies" applicable to other similar structures of arbitrary size. We demonstrate in Section 2 that bifurcation or non-bifurcation of a particular structure hinges upon whether a diffusion parameter R, analogous to the Reynolds number for neutral flows, exceeds a critical value. This R value provides an estimate for the scale size of the state of marginal bifurcation tendency. It also provides an estimate for the lifetime of the marginal state. We determine the critical R by high resolution numerical simulation of an isolated structure of relevant geometry. Just enough physical diffusion is added to prevent bifurcation and loss of resolution.

We are aware that mechanisms other than diffusion can affect structure on suitable scales. Among these are inertial forces, kinetic (finite gyroradius) effects, and E-to-F layer coupling. It is our desire, however, to present the most basic model which seems to agree with the stated observations. In order to explain the side-by-side existence at late times of

15 meter and kilometer scale sizes [Baker and Ulwick, 1978] we hypothesize that the cloud is dominated by turbulent diffusivity of order 100 m^2/sec, but that selected regions may reflect non turbulent electron diffusion of order 1 m^2/sec.

In Section 3 we describe the numerical techniques by which the equations of motion are solved. These techniques reflect appropriate advances in the state-of-the-art since the early simulations of large scale striation morphology [Zabusky, et al., 1973; Scannapieco, et al., 1974, 1976]. The scaling derived in Section 2 allows us to simulate a small region of the plasma with adequate resolution, providing that boundary conditions can be specified appropriately. Section 4 contains results of the numerical simulations and illustrates how the critical R depends upon the conductivity ratio M. In Section 5 we show that our calculated R values are compatible with rocket probe data on scales of tens of meters [Baker and Ulwick, 1978]. We show that if turbulent diffusivity is operative, a wide range of conditions will lead to marginally stable scale sizes of approximately one kilometer. In addition, we predict that the lifetime of the kilometer-scale structure should be of order 10^4 sec., in agreement with propagation experiments conducted during the STRESS program [Prettie et al., 1977]. Thus it is possible that our results may help to explain the "freezing up" of visible kilometer-scale barium cloud structures [J. A. Fedder, W. Chestnut, private communication, 1980].

2. Equations of Motion for the One Level Model

The two dimensional field line integrated Pedersen conductivity model appropriate to F-region clouds consists of the following equations (in cgs units) which are cast in a frame drifting with the ambient plasma:

$$\frac{\partial \Sigma}{\partial t} = - \nabla \cdot \Sigma \underline{V} + K \nabla^2 \Sigma \qquad (1)$$

$$\underline{V} = -\frac{c}{B} \nabla \phi \times \hat{\underline{z}} \tag{2}$$

$$\nabla \cdot \Sigma \nabla \phi = E_o \frac{\partial \Sigma}{\partial y} , \tag{3}$$

where Σ is the magnetic field-line-integrated Pedersen conductivity, K is the cross-field diffusivity of the cloud plasma, $\underline{V}$ is the local plasma drift relative to the ambient drift velocity, c is the speed of light, $\underline{B} = B\,\hat{\underline{z}}$ is the constant magnetic field strength, ϕ is the induced electrostatic potential, and $\underline{E}_o = E_o\,\hat{\underline{y}}$ is the ambient electric field in the rest frame of the neutral atmosphere. Equations (1) - (3) are two dimensional (x,y) where x is parallel to the relative neutral wind and y is the direction of $\underline{E}_o$. Except for the assumption of constant K, these equations are accurate to first order in the ratio of ion collision frequency to gyrofrequency. Equation (1) results from multiplying the ion continuity equation by the Pedersen mobility and integrating along the magnetic field. One assumes that the electrostatic potential and therefore $\underline{V}$ are constant on field lines. The diffusion term in (1) results from the assumption of a constant Pedersen mobility and K value within the cloud. The assumption of constant K is admittedly simplistic. For a typical barium cloud without turbulence, K is roughly proportional to the local plasma density [Perkins et al., 1973]. For a turbulent cloud, K may be scale size dependent [Goldman and Sperling, 1979]. Attempts to model the variation of K introduce an additional scaling parameter and tend to muddy the results without changing them significantly. Equation (3) is the equation of quasi-neutrality, which states that the field line integrated electric current, $\underline{J} = \Sigma\,\underline{E} = \Sigma(\underline{E}_o - \nabla\phi)$, must be divergence free.

For the sake of completeness, we should mention that a two layer model with one layer for the cloud and another for the background ionosphere has

been in use for several years [Lloyd and Haerendel, 1973]. One notices that simulations performed with the model tend to yield late time configurations in which there is a strong correlation between density distributions in the two layers [Scannapieco et al., 1976; S. T. Zalesak, private communication, 1980]. This may lend support to one level predictions concerning bifurcation of a particular structure, providing that the conductivity is dominated by the Pedersen component at the cloud level. Equations (1) - (3) may be put into dimensionless form as follows [McDonald, et al., 1978]. Let

$$\begin{aligned}
\underline{x} &= L_o \underline{x}' \\
dt &= t_o dt' \\
\Sigma &= \Sigma_o \Sigma' \\
\underline{V} &= V_o \underline{V}' \\
\phi &= L_o E_o \phi' \\
V_o &= c|E_o/B|,
\end{aligned} \tag{4}$$

and

$$t_o = L_o/V_o .$$

Here L_o is a measure of the cloud's gradient scale size, and all primed quantities are dimensionless. V_o is the relative drift speed between the ambient plasma and the neutral atmosphere, and Σ_o is the ambient integrated Pedersen conductivity. In this paper we take

$$L_o = (\int \Sigma^2 \, dx \, dy)^{\frac{1}{2}} / (\int (\nabla\Sigma)^2 \, dxdy)^{\frac{1}{2}} \tag{5}$$

where the region of integration is a rectangular box containing the structure of interest. We have experimented with more sophisticated definitions of L_o which are insensitive to the size of the box. These yield results within 20% of those given by (5) for the cases presented here. We prefer to retain the straightforward simplicity of (5).

Substituting (4) into (1) - (3) and dropping primes from all variables we have the dimensionless equations

$$\frac{\partial \Sigma}{\partial t} = - \nabla . \Sigma \underline{V} + R^{-1} \nabla^2 \Sigma \qquad (6)$$

$$\underline{V} = - \nabla \phi \times \hat{\underline{z}} \qquad (7)$$

$$\nabla . \Sigma \nabla \phi = \hat{\underline{y}} . \nabla \Sigma, \qquad (8)$$

where $$R = V_o L_o / K. \qquad (9)$$

Note that R is analogous to the Reynolds number for neutral flows, with the kinematic viscosity replaced by the cross-field plasma diffusivity.

Equations (6) - (8) reveal that the evolution of a plasma cloud is completely determined by initial cloud geometry, boundary conditions, and the value of R. Thus the answer to whether or not a given structure will bifurcate depends upon whether R is greater or smaller than some critical R value applicable to that structure. For sufficiently small R, diffusion will be dominant and will smooth out small structures faster than they can be created. For sufficiently large R, diffusion will be negligible, allowing steepening and bifurcation to proceed.

If the critical R for a particular structure is known, we can use (9) to estimate the scale size of the marginally stable state, providing estimates for V_o and K are available:

$$L_o = K\, R/V_o \qquad (10)$$

The lifetime of the marginal state may also be estimated. The time required for diffusion to degrade the structure is approximately

$$\begin{aligned} t_D &= L_o^2/K \\ &= R\, L_o/V_o \end{aligned} \tag{11}$$

One sees that t_D is R times the one dimensional gradient drift instability growth time. Anticipating that R is a large number, (11) implies that the marginal state can persist for times much greater than basic gradient drift structuring times.

In this work we investigate bifurcations which originate near the tips of striations. This seems to be the most likely place for new structure to emerge, although there is photographic evidence, for example in SPRUCE, that some new structure can emerge from sides of striations. The procedure for estimating the critical R for a given initial condition on Σ will be to carry out a set of simulations from equations (1) - (3) with assorted values of K. An upper limit on the critical R will be taken to be the smallest R at the time of first bifurcation. A lower limit will be taken as the largest R among non-bifurcating cases at times used to determine the upper limit. The initial condition on Σ will be taken as an appropriate form representing a single ated striation tip. This allows numerical resolution to be 4 to 8 times that of our earlier study [McDonald et al., 1978].

3. Numerical Simulations

Equations (1) - (3) are advanced in time using numerical techniques described below. A more detailed description of the NRL one-level striations code has been given by McDonald et al., [1979]. We choose the dimensional set rather than (6) - (8) to facilitate comparison with experiment.

With $\Sigma(x,y)$ given at a particular time, we calculate ϕ from (3), and use the result in (2) to arrive at the flow field $\underline{V}$. Then we use (1) to advance Σ by one timestep, after which the cycle can be reinitiated. Finite difference representations are used for all derivatives in (1) - (3).

Solution of the variable coefficient elliptic equation (3) accounts for nearly two-thirds of simulation time for grids as large as that used here (162 by 82 points). We use the Chebychev semi-iterative method to calculate a series of approximations which converge to the true solution of (3) [Varga, 1962; McDonald, 1980]. This method was chosen because of its efficient execution on a vector computer such as the NRL Texas Instruments ASC. It also allows convenient implementation of a wide variety of boundary conditions. Derivatives are represented by second order finite differences on a uniform, non-staggered grid (Σ, ϕ, and $\underline{V}$ are calculated on the same set of points). It is possible to obtain an exact solution to the finite difference analog of (3) [Madala, 1978], but computer time and storage requirements become excessive for large grids. We use time extrapolation to obtain an accurate initial approximation to ϕ , and carry out iterations until the root mean square residual error is approximately 3×10^{-4} of the root mean square source term. Reduction of the error much below this level would not necessarily improve results, since discretization introduces errors of this order or greater into the equations.

For the advection term in equation (1) we use the two dimensional flux correction method of Zalesak [1979]. This technique can be incorporated into a number of standard advection schemes to prevent formation of spurious oscillations in the advected quantity. There are two reasons why these oscillations should be avoided: (1) in a divergenceless flow field (see eq. (2)) new maxima or minima cannot be created: and (2) high order schemes can drive Σ negative, resulting in degeneracy of eq. (3) and physically

meaningless velocities. Traditional remedies include local "fill-in" and addition of artificial diffusion globally. The flux correction technique operates locally in regions where the oscillations tend to form, effectively truncating the scheme to first order such that ripples cannot form. The diffusion term in equation (1) is added in a separate step using second order spatial, forward time differencing. In the integration of equation (1) we tacitly subtract from $\underline{V}$ the structure's centroid velocity. This keeps the interesting structure from drifting off the computational grid. More important, it reduces the number of grid cells through which the structure drifts during a simulation. This helps to reduce discretization error due to the irreversible loss of information that occurs when an arbitrary profile is advected at constant velocity through an Eulerian grid.

The simulations were carried out on a grid of 162 by 82 points in the x and y directions respectively. Each simulation was carried out with a uniform grid interval of 80 meters and was then rerun with a grid interval of 40 meters as a check on the sensitivity of results to resolution. The use of a non-stretched grid increases execution efficiency of the code. The problems arising from electrostatic images on the boundaries are partially alleviated by the use of transmittive boundary conditions described below. The calculation procedure is to update quantities on the interior of the grid (160 x 80 points) by the methods described above, and then calculate exterior values from the boundary conditions.

Boundary conditions used during the simulation are as follows.

Neumann boundaries

$$\frac{\partial}{\partial n} = 0 \qquad (12)$$

(with n the outward normal) are imposed upon Σ and intermediate variables involved in updating equation (1). This allows inflow and outflow of ambient plasma on three sides of the grid where structure does not intersect the boundary (see Figures 1-4). It is also a good approximation for the fourth side (the left boundary of each figure) since Σ contours tend to align with the neutral wind direction (x) except near striation tips. For the present study, the Neumann condition seems more realistic than the periodic boundaries used in most earlier simulations. The "re entry" of plasma resulting from periodicity would be nonphysical in the study of an isolated structure.

The physically proper boundary condition on ϕ is that its gradient vanish at infinity. Since we are constrained to a grid of finite extent, we can either stretch the grid to move the boundary far from the structure or attempt to match the interior solution with an appropriate exterior solution. We have chosen an approximation to the second alternative and have developed a physically motivated algorithm which is admittedly simplistic, but has been validated empirically. Our approximate boundary condition is

$$\frac{\partial \phi}{\partial n} + S \frac{\partial^2 \phi}{\partial n^2} = 0 \qquad (13)$$

where n is the outward normal and S is a constant taken to be the cloud's initial scale size (see (15)). This states that the normal component of the polarization electric field must decrease in the outward direction on a spatial scale comparable to that of the gross structure. We choose to cast (13) in terms of the first two derivatives rather than ϕ and its first derivative so that the addition of a constant to ϕ would have no effect upon structure evolution. We have validated (13) by comparing analytic and finite difference solutions to (3) for elliptic "waterbag" distributions

$\Sigma\,(x,y)$. The condition (13) gave results superior to the usual periodic, Neumann, or Dirichlet boundaries.

Initial conditions for the simulations are taken to be descriptive of the tip of a striation (see upper portions of Figures 1-4). Taking the origin at the center of the rectangular grid, we have at $t = 0$

$$\begin{aligned} \Sigma &= 1 + (M-1)\,\exp(-y^2/S^2),\ x < 0 \\ &= 1 + (M-1)\,\exp(-(x^2+y^2)/S^2,\ x \geq 0 \end{aligned} \tag{14}$$

where M is the ratio of peak conductivity to ambient. For all cases presented here,

$$S = 1\ \text{km}\ . \tag{15}$$

The computational domain for results shown in Figures 1-4 is 6.4 by 12.8 kilometers. That we have normalized Σ to the ambient Σ_o has no effect on the model (1) - (3) (i.e., Σ can be replaced with Σ/Σ_o). All other variables retain their dimensionality. For all cases we take B = .5 gauss, and $E_o = -1.67 \times 10^{-7}$ stat volts/cm, so that V_o = 100 m/s. In this particular simulation it is not necessary to perturb the initial condition, since (14) does not represent a steady state. One must note, however, that discretization and roundoff errors provide effective pertubations to any simulation.

4. Results

Simulation results used to determine upper and lower limits on R for each of four M values (2, 5, 10, and 30) are shown in Figures 1-4. For each M, a set of simulations were carried out for various K values in order

to help locate the demarcation between bifurcating and non bifurcating states. For each M value we present the two simulations which most accurately bound the critical R. In each case this involves a pair of K values separated by a factor of 2. The range could be narrowed by further simulations, but the approximations involved in taking K constant and specifying boundary conditions at finite distances would lend some uncertainty to the result. Our earlier critical R value for an M = 11 structure [McDonald et al., 1978] is approximately a factor of 2 lower than one would expect from the present work (see Figure 6). We attribute this to the use of different initial conditions, boundary conditions, lower spatial resolution, and a different procedure for determining the critical R.

In each of Figures 1-4 the left column gives contour plots of Σ for cases where K is small enough to permit bifurcation. The plot just below the initial condition plot shows Σ at a time when it is qualitatively clear that bifurcation is about to occur. This time is chosen as appropriate to determine the critical R from (5) and (9). We choose not to determine R at t = 0 because the uniform separation of contours is not "natural." This becomes clear when one examines the non bifurcating states in the right column of Figures 1-4. A quasi stationary state is established only after a sufficient amount of steepening has occurred. It is the stability of a pre-steepened and thus more "natural" state that we wish to address. When the structure is near bifurcation, the selection of a time for calculating R is not crucial. As shown in Figure 5, the length scale tends to level off just prior to the development of new structure. Thus our results are not sensitive to the precise definition of an onset time.

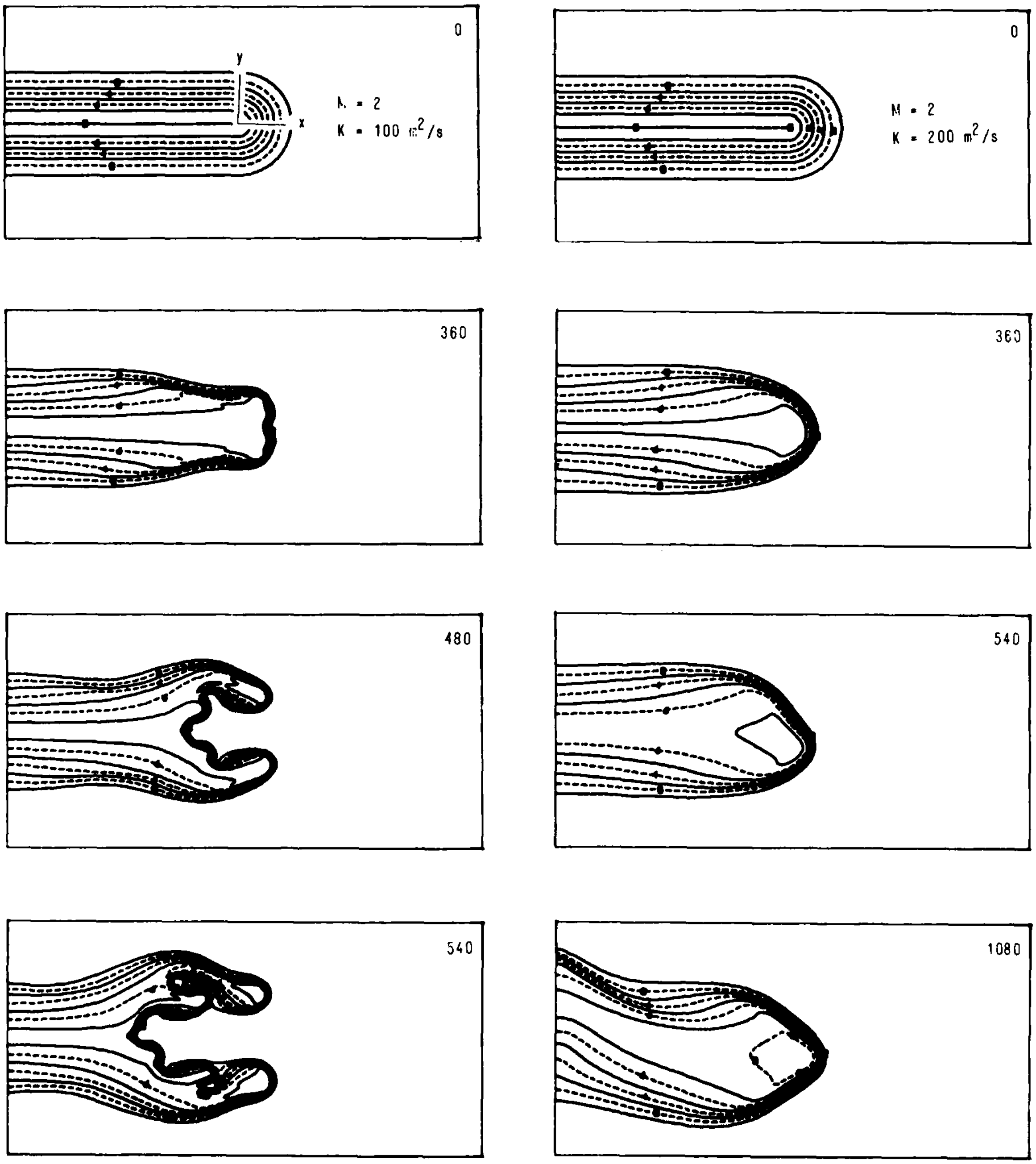

Fig. 1 — Contour plots of $\Sigma(x,y)$ at selected times illustrating the demarcation between bifurcating (left column) and non-bifurcating (right column) states for M = 2. Contours are spaced linearly between $\Sigma = 1$ (ambient) and M. Limits on the critical R are evaluated at times when bifurcation of the low K striation (second plot in left column for Figures 1—4) is eminent. Times appear in the upper right of each plot.

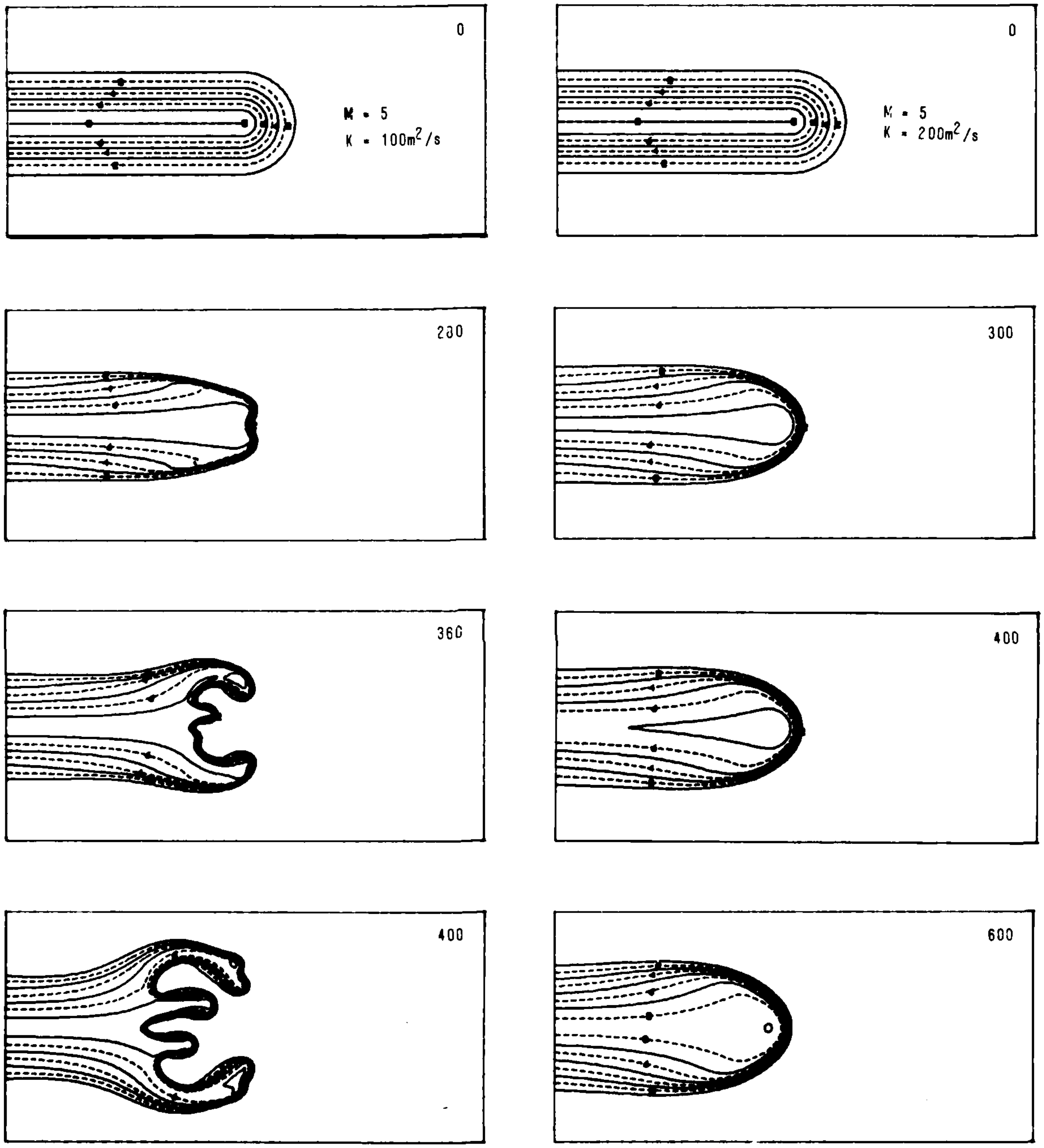

Fig. 2 — Contour plots of $\Sigma(x,y)$ at selected times illustrating the demarcation between bifurcating (left column) and non-bifurcating (right column) states for M = 5. The diffusion dominated case is plotted at 300 seconds, the time at which L_0 attains a shallow minimum (see Figure 5). Past this time diffusive dominance is evidenced by the drying up of inner contours.

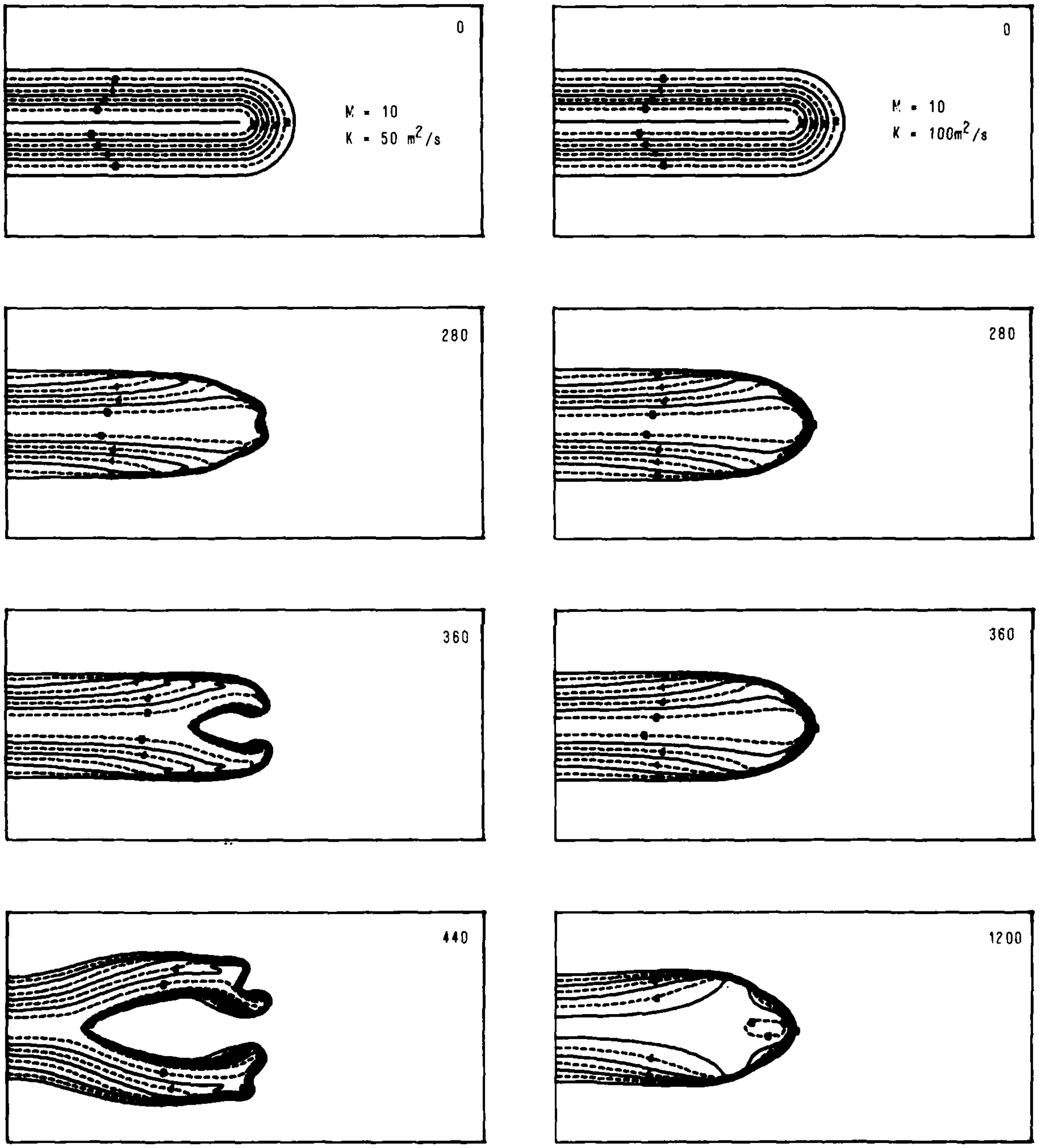

Fig. 3 — Contour plots of $\Sigma(x,y)$ at selected times illustrating the demarcation between bifurcating (left column) and non-bifurcating (right column) states for M = 10. Contours are spaced linearly between $\Sigma = 1$ (ambient) and M. Limits on the critical R are evaluated at times when bifurcation of the low K striation (second plot in left column for Figures 1—4) is eminent. Times appear in the upper right of each plot.

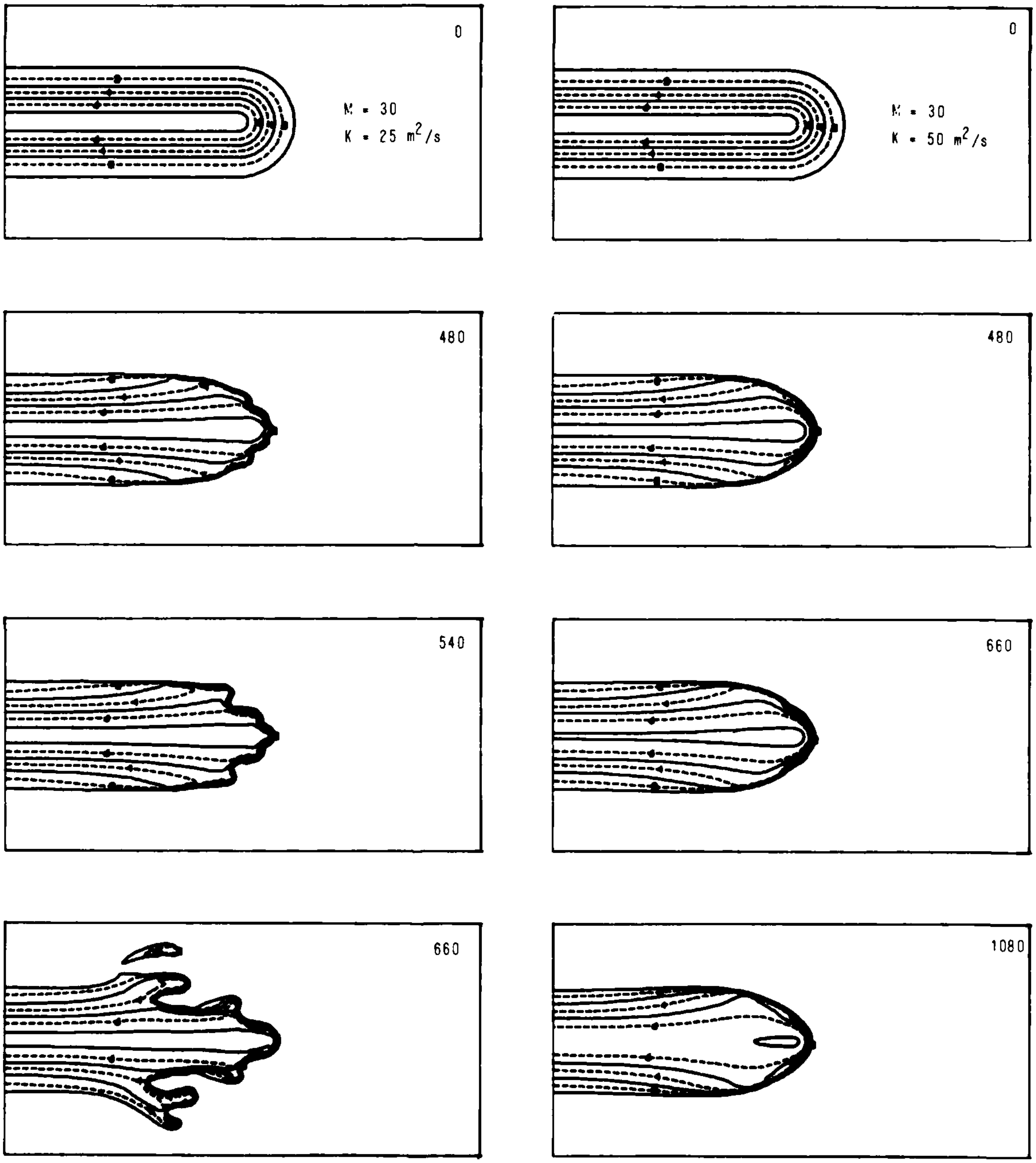

Fig. 4 — Contour plots of $\Sigma(x,y)$ at selected times illustrating the demarcation between bifurcating (left column) and non-bifurcating (right column) states for M = 30. Contours are spaced linearly between $\Sigma = 1$ (ambient) and M. Limits on the critical R are evaluated at times when bifurcation of the low K striation (second plot in left column for Figures 1—4) is eminent. Times appear in the upper right of each plot.

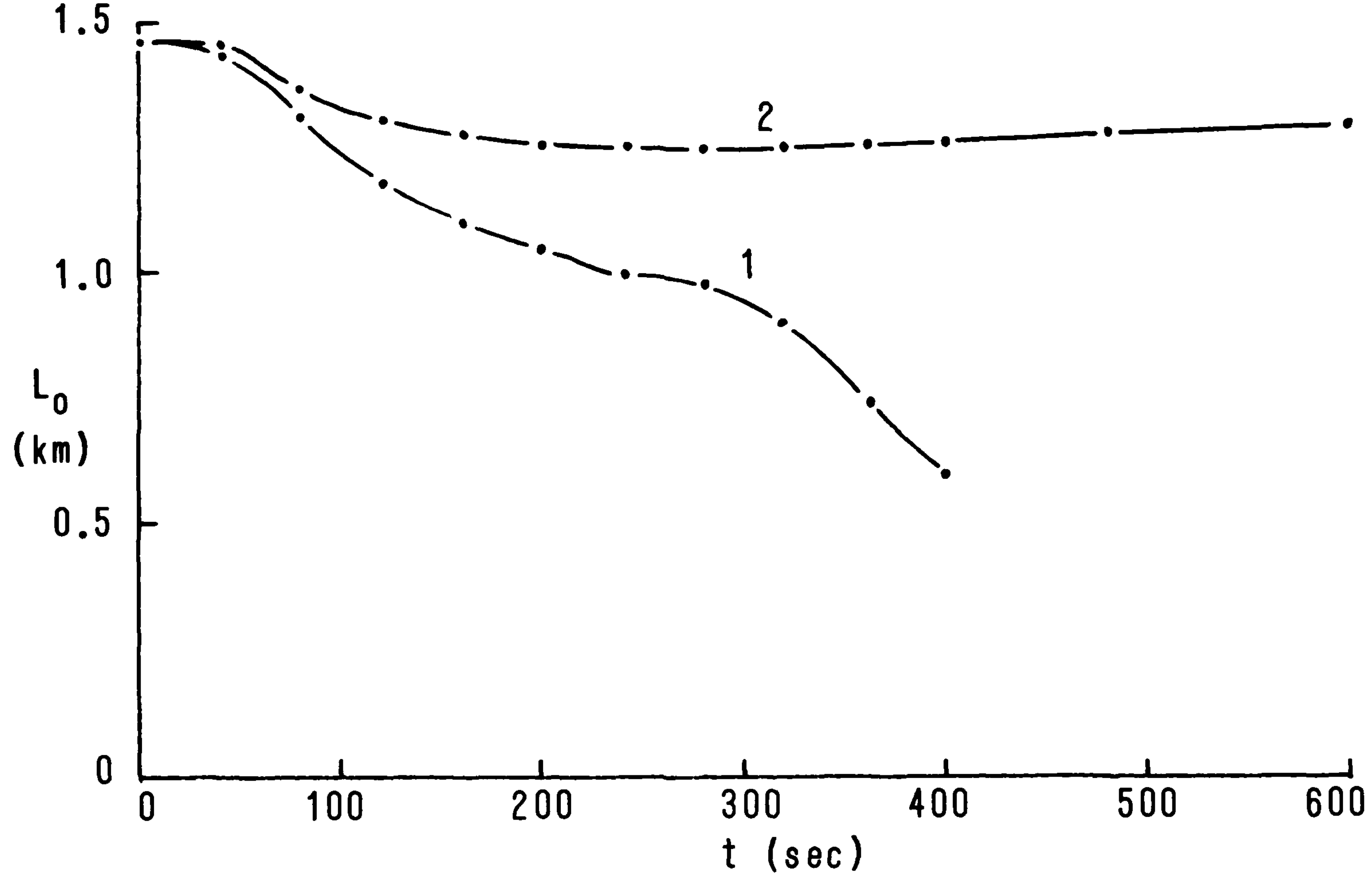

Fig. 5 — L_o vs time for Figure 2. Curve 1 is the bifurcating case, and curve 2 is the non-bifurcating case

Curves 1 and 2 of Figure 5 shows L_o as a function of time for the M = 5 simulations. Both curves show an initial transient for $0 \leq t \lesssim 125$ sec, indicating that the initial condition is far from a "natural" quasistationary state. For $125 \leq t \lesssim 300$ sec, curve 1 shows L_o slowly decreasing, corresponding to the well known backside steepening phenomenon. Then for t > 300 sec, L_o decreases rapidly, indicating the onset of bifurcation. This abrupt change in the slope of $L_o(t)$ coincides with bifurcation in all our runs. In contrast, curve 2 of Figure 5 shows L_o settling down to a nearly constant value after the transient period. L_o reaches a shallow minimum at 300 sec., indicating the onset of diffusive dominance rather than bifurcation. The coincidence of this minimum with the knee in curve 1 is fortuitous, since the minimum can be made to occur earlier by increasing the diffusivity.

The bounds on critical R values gleaned from the simulations are given in Table 1. The column denoted "resolution" refers to results from Figures 1-4 and a duplicate set of simulations performed with twice the spatial resolution on the 162 x 82 grid (boundaries are placed closer to the structure). The degree to which upper and lower bounds are different for different spatial resolution gives a measure of discretization and boundary effects. The geometric means of all R values from Table 1 are 1207 and 1355 for high and low resolution, respectively, and differ by only 11%. The geometric mean of upper and lower bounds for a given M is plotted as a function of M in Figure 6. This plot suggests that the critical R attains a minimum value between 600 and 700 for $M \cong 4$.

Table 1 — Critical R vs. Conductivity Ratio

M	Resolution	Range			Geometric Mean
2	High	1629	> R . >	993	1561
	Low	2402		1527	
5	H	769		450	676
	L	971		623	
10	H	1110		692	987
	L	1450		853	
30	H	4440		2310	2552
	L	2722		1519	

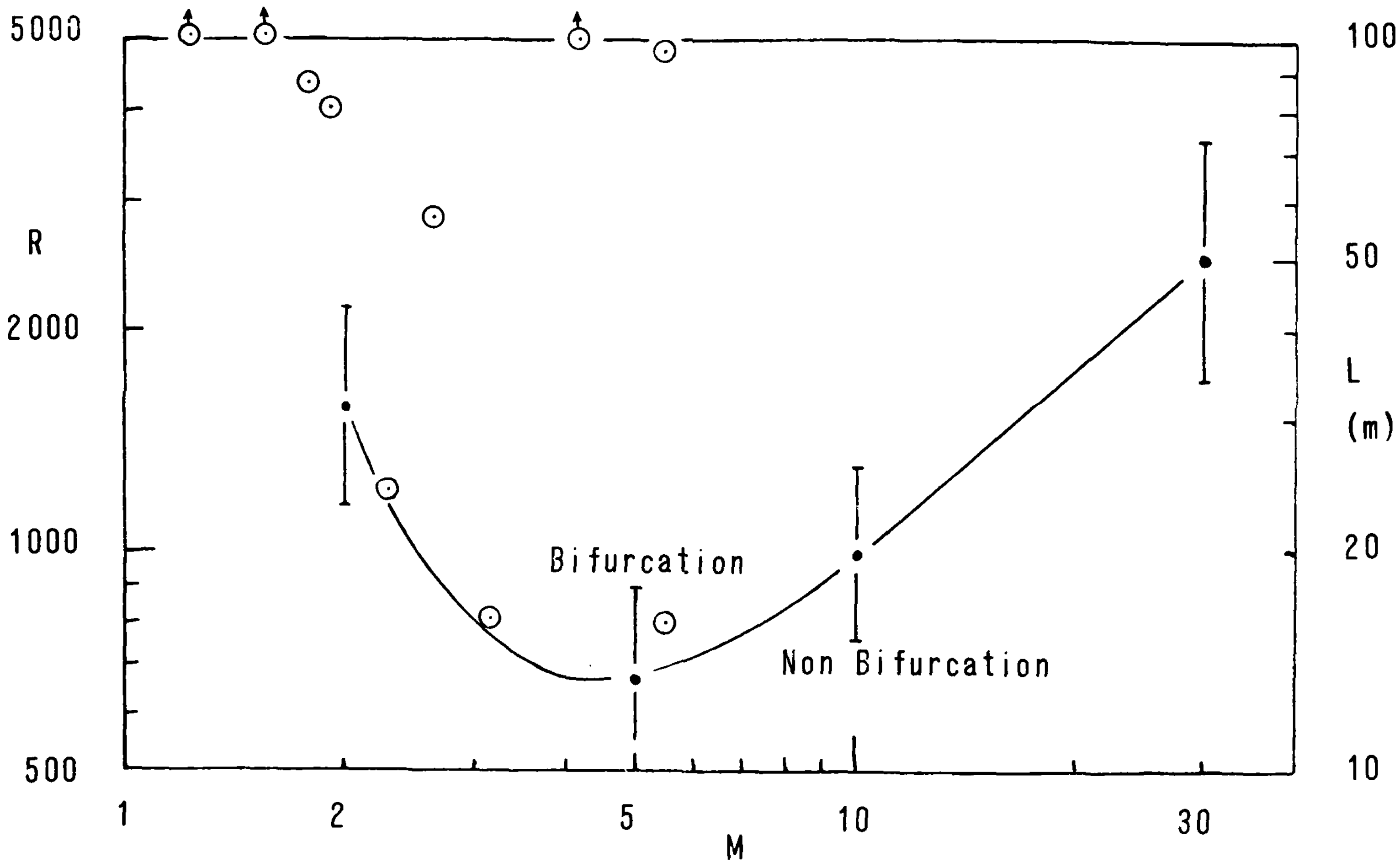

Fig. 6 — Critical R vs M. Solid points: mean values from Table 1. Error bars denote log variances. Circled points: density falloff scale size L vs M from rocket data for event Esther [Table 5.1 of Baker et al., 1978].

The shape of this curve is a gratifying result which lends support to the simulations. Linson [1975] offered an ad hoc model to explain observed onset times as a function of M. This model, based on slip velocities for elliptical piecewise constant density ("waterbag") clouds, predicted a U-shaped curve with a minimum onset time for some $M > 2$, the exact value depending on the shape of the cloud. This model was found qualitatively consistent with simulation results for realistic cloud profiles [McDonald et al., 1980]. This minimum onset time may be viewed as a maximum bifurcation tendency. The amount of diffusion required to halt bifurcation is thus maximum at some M value, resulting in a minimum critical R. A recent result of Overman and Zabusky [1980] for circular waterbag clouds also supports the qualitative dependence of the critical R upon M as shown in Figure 6. They find that shielding and dissipation cooperate so as to produce an effective diffusivity which is the actual diffusivity times $(M+1)^2/(M-1)$. If we assume that the amount of effective diffusivity required to halt bifurcation is insensitive to M, the critical R should be proportional to $(M+1)^2/(M-1)$. This expression has a minimum at $M = 3$, in approximate agreement with the curve of Figure 6. In fact, with the exception of the $M = 2$ case, the expression $R = 75\ (M+1)^2/(M-1)$ gives the mean R values of Table 1 to 3% accuracy. For high M, the polarization charges responsible for shielding reside in a thin layer in which the cloud's conductivity rises from ambient to a few times the ambient value. The thinness of this layer results in agreement of the cloud's polarization electric field with that of a suitable waterbag cloud.

Other data from the simulations are presented in Table 2. The marginally stable structures in the right columns of Figs. 1-4 have been Fourier analyzed at times at which the critical R is evaluated. Summing the two dimensional spectral power over the transverse wavenumber yields one dimen-

sional in situ power spectra $P(k_x) \propto k_x^{-n_x}$ and $P(k_y) \propto k_y^{-n_y}$ for the x and y directions respectively. The proportionality is valid only in the central portion of the spectrum. Diffusive dominance is evident in the steepness of the y spectra as compared to the x spectra. This suggests the possibility that a rocket moving transverse to the neutral wind through a "frozen" cloud might find a power spectral density steeper by one or two powers of k than a rocket moving parallel to the neutral wind (assuming that turbulent fluctuations can be removed from the data). Finally, the coupling coefficient ζ is given which is simply the ratio of striation centroid velocity V_c to ambient plasma drift speed V_o in the frame of the neutral atmosphere. In agreement with analytic results from a waterbag model [Linson, 1975], ζ is roughly proportional to M^{-1} as a result of electric field shielding at high M.

Figures 1-4 reveal that the manner in which an unstable structure comes apart is dependent on the conductivity ratio. For $M \lesssim 10$, depletions are able to penetrate the initial structure with ease. However, for $M \gtrsim 10$, there is a tendency for the secondary structure to be confined to the surface of the original structure. High conductivity clouds are peeled like an onion, while low conductivity clouds are cut like an apple. This effect is even more apparent in our earlier work [McDonald et al., 1980].

Table 2 — Spectral Indices and Centroid Drifts for Marginally Stable States

M	TIME	n_x	n_y	$\zeta = (V_c-V_o)/V_o$
2	360	2.2	5.4	0.634
5	280	1.8	4.2	0.305
10	280	1.8	3.1	0.160
30	480	2.0	3.1	0.057

5. Summary and Comparison with Data

For plasma structures resembling striation tips, the model (1) - (3) implies that the demarcation between bifurcating and non bifurcating states is determined by the value of R (analogous to the Reynolds number in hydrodynamics) and the conductivity ratio M. This demarcation has been estimated by computer simulation and is presented in Figure 6. The critical R reaches a minimum of roughly 700 for $M \approx 4$. Its dependence upon M is similar to that of the onset time for striation emergence from a two dimensional cloud [Linson, 1975; McDonald et al., 1980]. This similarity is a result of bifurcation tendency being offset by a proportional amount of diffusion.

Our results compare favorably with three distinct types of experimental observations. These are a) minimum scale sizes as determined by rocket probe data; b) the "freezing-up" of visible structure on scales of approximately one kilometer; and c) the lifetime of the "frozen" state. We shall now discuss each of these areas.

A. Minimum Scale Sizes

If M is known for a structure, we can find the critical R from the curve of Figure 6. We can then use (10) to estimate L_o, providing we have estimates for V_o and K. Since L_o is proportional to K, one expects the smallest scales to be determined by the classical (non turbulent) diffusivity

$$K = 2 \frac{\nu_e}{\Omega_e} \frac{ckT}{eB} , \qquad (16)$$

where ν_e is the sum of electron collision frequencies with cloud ions and ambient neutrals, Ω_e is the electron gyrofrequency, k is Boltzmann's constant, T is the plasma temperature, and e is the electron charge. The expression (16) is equivalent to that used in eq. (22) of Perkins et al. [1973].

For plasma number densities $n \gtrsim 3 \times 10^5$ cm^{-3} at altitudes of 150 km or greater, ν_e is dominated by ionic collisions. Thus K varies approximately as $nT^{-\frac{1}{2}} B^{-2}$, as a result of the following.

$$\nu_e \approx \nu_{ei} = (34 + 4.18 \log_{10}(T^3/n)) \, nT^{-3/2}, \qquad (17)$$

where n is in cm^{-3}, T is in ^oK, and ν_e is in sec^{-1}. High resolution plasma probe data for the barium cloud Esther [Figure 2 of Baker and Ulwick, 1978] at approximately 170 km give $5 \times 10^6 \geq n \geq 3 \times 10^5$ cm^{-3}. We have from (16) and (17) with T = 1000 ^oK,

$$\begin{aligned} K &= 0.182 \ m^2/s, \quad n = 3 \times 10^5 \ cm^{-3} \\ &= 2.71 \ m^2/s, \quad n = 5 \times 10^6 \ cm^{-3} \end{aligned} \qquad (18)$$

In order to estimate M for individual striations in the cloud, we need Σ values in the ambient ionosphere and throughout the cloud (denoted by Σ_a and Σ_c, respectively). Taking a magnetic dip angle I = 61.5^o for Eglin AFB, Florida, Francis and Perkins [1975] give for the twilight ionosphere

$$\Sigma_a \approx 3.5 \text{ mho} \qquad (19)$$

Since the cloud is contained well above 125 km (where $\nu_i/\Omega_i \approx 1$ for B_a^+) we can take

$$\Sigma_c = \frac{ec}{B} \int n_c \, \nu_i/\Omega_i \, dh \csc I, \qquad (20)$$

where the path of integration is along the magnetic field, h is altitude, and field line curvature is neglected. Use of altitude rather than distance along the field facilitates comparison with data. Assuming

$$n_c = n_o \exp(-h^2/D^2),$$

$$\nu_i = \nu_o \exp(-h/H),$$

(20) gives

$$\Sigma_c = D \quad n_o \quad \frac{ec}{B} \frac{\nu_o}{\Omega_i} \quad \csc I \quad \pi^{\frac{1}{2}} \exp(D^2/4H^2). \qquad (21)$$

Zero subscripts refer to values at the cloud peak along a given field line. For conditions applicable to 170 km altitude at sunset, the result of Linson and Baxter [1977] for B_a^+ gives ν_o/Ω_i = .0749 and H = 25.0 km. Taking B = .5G, and D = 17.31 km corresponding to Esther's full width at half maximum [Baker and Ulwick, 1978] of 24 km, (21) gives

$$\Sigma_c = n_o \ (cm^{-3}) \times 9.433 \times 10^{-6} \ \text{mho}$$

The measured values $5 \times 10^6 \geq n \geq 3 \times 10^5 \ cm^{-3}$ give

$$47.2 \geq \Sigma_c \geq 2.83 \ \text{mho}. \qquad (23)$$

M values for the individual striations in the Esther cloud are taken to be ratios of $\Sigma = \Sigma_a + \Sigma_c$ for neighboring peaks and valleys as given by Table 5.1 of Baker et al. [1978]. Scale sizes L for density falloff are given in this table and are plotted as circled points in Figure 6. One sees that minimum scale sizes for a given M are in agreement with our simulation results, providing we take

$$K/V_o = 0.02 \ \text{meter}. \qquad (24)$$

With V_o = 100 m/s, we have K = 2 m^2/s, in agreement with the range given by (18). The existence of scale sizes well above the curve of Fig. 6 could be a result of oblique cuts through shanks rather than tips of striations. It could also be a result of an enhanced diffusivity (to be discussed below), lack of complete temporal development, or effects not included in the model (as mentioned in Sec. 1).

B. Kilometer Scale Visible Structure

Departing the issue of minimum scale sizes which seem to be controlled by classical diffusion, our results can be used to address the frequent emergence of visible structure with scale sizes of order 1 kilometer. We hypothesize that plasma turbulence may be involved in these structures. This admits the possibility of individual parcels of plasma macroscopically acting as agents of fluid transport, while microscopically being subject to classical particle diffusion. Thus the smallest structures may reflect electron diffusion dominance, while much larger structures may reflect enhanced diffusivity effects. In order to model these large scale structures, we replace the classical particle diffusivity (16) by an enhanced diffusion term descriptive of a turbulent process. Our goal is not to prove that turbulence is operative, but to offer at least <u>one</u> physically plausible explanation for observed scale sizes and lifetimes.

If we take Bohm diffusion [Chen, 1974]

$$K_B = \frac{1}{16} \frac{ckT}{eB} \tag{25}$$

as descriptive of turbulent diffusivity, we find K values much greater than those given by (16) for typical barium releases. With $T = 1000^oK$ and $B = .5$ G, (25) gives $K_B = 108\ m^2/s$. The curve in Figure 6 suggests that $R \approx 1000$ is accurate to $\pm$ 30% for a range of M values from approximately 2 to 15. Thus (9) would predict $L_o \approx 1$ km for the gradient scale size for a variety of typical barium releases in which $V_o \approx 100$ m/s. This in agreement with observations cited in the Introduction [J. A. Fedder, W. Chestnut, private communication, 1980].

C. Lifetime of the Kilometer Scale Structure

If the persistent structure is viewed as marginally stable to bifurcation, its lifetime will be determined by diffusion, and should be in approximate agreement with (11). Using L_o = 1km and K_B = 100 m^2/s, we find a diffusion time scale of 10^4 sec. = 2.7 hours. Horizontal drift and sunlighting conditions make visual tracking of a cloud for this length of time very difficult. However, satellite communications experiments have been conducted for timescales on this order during the STRESS program. For the five STRESS releases, propagation through the clouds resulted in signal fading for durations of 1.4 to 3.7 hours after release [Prettie et al. 1977]. The beam frequency of 341 MHz and the approximate 200 km range from cloud to receiving aircraft implies that the fading was sensitive to structure on scales roughly that of the Fresnel size $(\lambda z)^{1/2}$ = 420 meters.

Acknowledgment. This work was supported by the Defense Nuclear Agency.

References

Baker, K. D., J. C. Ulwick, M. C. Kelley, L. C. Howlett, G. D. Allred, D. Delorey, and N. Grossbard, Electron Density Structure in Barium Clouds - Measurements and Interpretation, Final Report, Contract No. DNA 001-76-C-0278, Utah State University, Logan, Utah, February, 1978.

Baker, K. D., and J. C. Ulwick, Measurements of electron density structure in striated barium clouds, _Geophys. Res. Lett._ _5_, 723, 1978.

Chen, F. F., _Introduction to Plasma Physics_, Plenum Press, New York, 1974.

Francis, S. H., and F. W. Perkins, Determination of striation scale sizes for plasma clouds in the ionosphere, _J. Geophys. Res._ _80_, 3111, 1975.

Goldman, S. R., and J. L. Sperling, Aspects of late time striation behavior and satellite communication effects, Final Report, Contract No. DNA 001-76-C-P00005, JAYCOR, Inc., Del Mar, California, January 1979.

Linson, L. M., Slab release and onset time of striatons; in Multiple barium release studies, KMR ionospheric monitoring program, Spring, 1975, _HAPREX Final Report V.3_, Stanford Research Institute, Menlo Park, California, October, 1975.

Linson, L. M., and D. C. Baxter, Ion cloud modeling, Final Report, Contract No. DNA 001-76-C-0274, Science Applications, Inc., LaJolla, California, November, 1977.

Linson, L. M., and J. B. Workman, Formation of striations in ionospheric plasma clouds. _J. Geophys. Res._ _75_, 3211, 1970.

Lloyd, K.H. and G. Haerendel, Numerical modeling of the drift and deformation of ionospheric plasma clouds and of their interaction with other layers of the ionosphere, _J. Geophys. Res._, _78_, 7389, 1973.

Madala, R. V., An efficient direct solver for separable and nonseparable elliptic equations, _Mon. Weather Rev._, _106_, 1735, 1978.

McDonald, B. E. The Chebychev method for solving nonself adjoint elliptic equations on a vector computer, J. Comp. Phys. 35, 147, 1980.

McDonald, B. E., S. L. Ossakow, S. T. Zalesak, and N. J. Zabusky, Determination of minimum scale sizes in plasma cloud striations, Proc. Symp. on Effect of the Ionosphere on Space and Terrestrial Systems, ed. J. M. Goodman, U.S. Government Printing Office, Stock No. 008-051-00069-1, 1978.

McDonald, B. E., S. L. Ossakow, S. T. Zalesak, and N. J. Zabusky, Simulation of gradient-drift striations on the ASC, Proc. Scientific Computer Information Exchange Meeting, Office of Basic Energy Sciences, Livermore, California, September 1979.

McDonald, B. E., M. J. Keskinen, S. L. Ossakow, and S. T. Zalesak, Computer simulation of gradient drift instability processes in operation Avefria, J. Geophys. Res. 85, 2143, 1980.

Overman, E.A. II, and N. J. Zabusky, Ionospheric plasma cloud (deformable dielectric) stability and nonlinear evolution via regularized contour dynamics, Department of Mathematics and Statistics, University of Pittsburgh, Technical Report ICMA-80-19, July 1980, Pittsburgh, Pa.

Perkins, F. W., N. J. Zabusky, and J. H. Doles III, Deformation and striation of plasma clouds in the ionosphere, 1, J. Geophys. Res., 78, 697, 1973.

Prettie, C., A. Johnson, J. Marshall, T. Grizinski, and R. Swanson, Project STRESS satellite communication test results, Air Force Avionics Laboratory, Wright-Patterson AFB, Ohio, Technical Report 77-158, July, 1977.

Scannapieco, A. J., S. L. Ossakow, D. L. Book, B. E. McDonald, and S. R. Goldman, Conductivity ratio effects on the drift and deformation of F region barium clouds coupled to the E region ionosphere, J. Geophys. Res., 79, 2913, 1974.

Scannapieco, A. J., S. L. Ossakow, S. R. Goldman and J. M. Pierre, Plasma cloud late time striation spectra, J. Geophys. Res. 81, 6037, 1976.

Varga, R. S. Matrix Iterative Analysis, Prentice Hall, Englewood Cliffs, N.J., 1962.

Zabusky, N. J., J. H. Doles III, and F. W. Perkins, Deformation and striation of plasma clouds in the ionosphere, 2. Numerical simulation of a non-linear two-dimensional model, J. Geophys. Res., 78, 711, 1973.

Zalesak, S. T., Fully Multidimensional flux-corrected transport algorithms for fluids, J. Comp. Phys. 31, 335, 1979.

DISTRIBUTION LIST

DEPARTMENT OF DEFENSE

ASSISTANT SECRETARY OF DEFENSE
COMM, CMD, CONT & INTELL
WASHINGTON, D.C. 20301
01CY ATTN J. BABCOCK
01CY ATTN M. EPSTEIN

ASSISTANT TO THE SECRETARY OF DEFENSE
ATOMIC ENERGY
WASHINGTON, D.C. 20301
01CY ATTN EXECUTIVE ASSISTANT

DIRECTOR
COMMAND CONTROL TECHNICAL CENTER
PENTAGON RM BE 685
WASHINGTON, D.C. 20301
01CY ATTN C-650
01CY ATTN C-312 R. MASON

DIRECTOR
DEFENSE ADVANCED RSCH PROJ AGENCY
ARCHITECT BUILDING
1400 WILSON BLVD.
ARLINGTON, VA. 22209
01CY ATTN NUCLEAR MONITORING RESEARCH
01CY ATTN STRATEGIC TECH OFFICE

DEFENSE COMMUNICATION ENGINEER CENTER
1860 WIEHLE AVENUE
RESTON, VA. 22090
01CY ATTN CODE R820
01CY ATTN CODE R410 JAMES W. MCLEAN
01CY ATTN CODE R720 J. WORTHINGTON

DIRECTOR
DEFENSE COMMUNICATIONS AGENCY
WASHINGTON, D.C. 20305
(ADR CNWDI: ATTN CODE 240 FOR)
01CY ATTN CODE 101B

DEFENSE TECHNICAL INFORMATION CENTER
CAMERON STATION
ALEXANDRIA, VA. 22314
(12 COPIES IF OPEN PUBLICATION, OTHERWISE 2 COPIES)
12CY ATTN TC

DIRECTOR
DEFENSE INTELLIGENCE AGENCY
WASHINGTON, D.C. 20301
01CY ATTN DT-1B
01CY ATTN DB-4C E. O'FARRELL
01CY ATTN DIAAP A. WISE
01CY ATTN DIAST-5
01CY ATTN DT-1BZ R. MORTON
01CY ATTN HQ-TR J. STEWART
01CY ATTN W. WITTIG DC-7D

DIRECTOR
DEFENSE NUCLEAR AGENCY
WASHINGTON, D.C. 20305
01CY ATTN STVL
04CY ATTN TITL
01CY ATTN DDST
03CY ATTN RAAE

COMMANDER
FIELD COMMAND
DEFENSE NUCLEAR AGENCY
KIRTLAND AFB, NM 87115
01CY ATTN FCPR

DIRECTOR
INTERSERVICE NUCLEAR WEAPONS SCHOOL
KIRTLAND AFB, NM 87115
01CY ATTN DOCUMENT CONTROL

JOINT CHIEFS OF STAFF
WASHINGTON, D.C. 20301
01CY ATTN J-3 WWMCCS EVALUATION OFFICE

DIRECTOR
JOINT STRAT TGT PLANNING STAFF
OFFUTT AFB
OMAHA, NB 68113
01CY ATTN JLTW-2
01CY ATTN JPST G. GOETZ

CHIEF
LIVERMORE DIVISION FLD COMMAND DNA
DEPARTMENT OF DEFENSE
LAWRENCE LIVERMORE LABORATORY
P. O. BOX 808
LIVERMORE, CA 94550
01CY ATTN FCPRL

DIRECTOR
NATIONAL SECURITY AGENCY
DEPARTMENT OF DEFENSE
FT. GEORGE G. MEADE, MD 20755
01CY ATTN JOHN SKILLMAN R52
01CY ATTN FRANK LEONARD
01CY ATTN W14 PAT CLARK
01CY ATTN OLIVER H. BARTLETT W32
01CY ATTN R5

COMMANDANT
NATO SCHOOL (SHAPE)
APO NEW YORK 09172
01CY ATTN U.S. DOCUMENTS OFFICER

UNDER SECY OF DEF FOR RSCH & ENGRG
DEPARTMENT OF DEFENSE
WASHINGTON, D.C. 20301
01CY ATTN STRATEGIC & SPACE SYSTEMS (OS)

WWMCCS SYSTEM ENGINEERING ORG
WASHINGTON, D.C. 20305
01CY ATTN R. CRAWFORD

COMMANDER/DIRECTOR
ATMOSPHERIC SCIENCES LABORATORY
U.S. ARMY ELECTRONICS COMMAND
WHITE SANDS MISSILE RANGE, NM 88002
01CY ATTN DELAS-EO F. NILES

DIRECTOR
BMD ADVANCED TECH CTR
HUNTSVILLE OFFICE
P. O. BOX 1500
HUNTSVILLE, AL 35807
01CY ATTN ATC-T MELVIN T. CAPPS
01CY ATTN ATC-O W. DAVIES
01CY ATTN ATC-R DON RUSS

PROGRAM MANAGER
BMD PROGRAM OFFICE
5001 EISENHOWER AVENUE
ALEXANDRIA, VA 22333
01CY ATTN DACS-BMT J. SHEA

CHIEF C-E SERVICES DIVISION
U.S. ARMY COMMUNICATIONS CMD
PENTAGON RM 1B269
WASHINGTON, D.C. 20310
01CY ATTN C-E-SERVICES DIVISION

COMMANDER
FRADCOM TECHNICAL SUPPORT ACTIVITY
DEPARTMENT OF THE ARMY
FORT MONMOUTH, N.J. 07703
01CY ATTN DRSEL-NL-RD H. BENNET
01CY ATTN DRSEL-PL-ENV H. BOMKE
01CY ATTN J. E. QUIGLEY

COMMANDER
HARRY DIAMOND LABORATORIES
DEPARTMENT OF THE ARMY
2800 POWDER MILL ROAD
ADELPHI, MD 20783
(CNWDI-INNER ENVELOPE: ATTN: DELHD-RBH)
01CY ATTN DELHD-TI M. WEINER
01CY ATTN DELHD-RB R. WILLIAMS
01CY ATTN DELHD-NP F. WIMENITZ
01CY ATTN DELHD-NP C. MOAZED

COMMANDER
U.S. ARMY COMM-ELEC ENGRG INSTAL AGY
FT. HUACHUCA, AZ 85613
01CY ATTN CCC-EMEO GEORGE LANE

COMMANDER
U.S. ARMY FOREIGN SCIENCE & TECH CTR
220 7TH STREET, NE
CHARLOTTESVILLE, VA 22901
01CY ATTN DRXST-SD
01CY ATTN R. JONES

COMMANDER
U.S. ARMY MATERIEL DEV & READINESS CMD
5001 EISENHOWER AVENUE
ALEXANDRIA, VA 22333
01CY ATTN DRCLDC J. A. BENDER

COMMANDER
U.S. ARMY NUCLEAR AND CHEMICAL AGENCY
7500 BACKLICK ROAD
BLDG 2073
SPRINGFIELD, VA 22150
01CY ATTN LIBRARY

DIRECTOR
U.S. ARMY BALLISTIC RESEARCH LABS
ABERDEEN PROVING GROUND, MD 21005
01CY ATTN TECH LIB EDWARD BAICY

COMMANDER
U.S. ARMY SATCOM AGENCY
FT. MONMOUTH, NJ 07703
01CY ATTN DOCUMENT CONTROL

COMMANDER
U.S. ARMY MISSILE INTELLIGENCE AGENCY
REDSTONE ARSENAL, AL 35809
01CY ATTN JIM GAMBLE

DIRECTOR
U.S. ARMY TRADOC SYSTEMS ANALYSIS ACTIVITY
WHITE SANDS MISSILE RANGE, NM 88002
01CY ATTN ATAA-SA
01CY ATTN TCC/F. PAYAN JR.
01CY ATTN ATAA-TAC LTC J. HESSE

COMMANDER
NAVAL ELECTRONIC SYSTEMS COMMAND
WASHINGTON, D.C. 20360
01CY ATTN NAVALEX 034 T. HUGHES
01CY ATTN PME 117
01CY ATTN PME 117-T
01CY ATTN CODE 5011

COMMANDING OFFICER
NAVAL INTELLIGENCE SUPPORT CTR
4301 SUITLAND ROAD, BLDG. 5
WASHINGTON, D.C. 20390
01CY ATTN MR. DUBBIN STIC 12
01CY ATTN NISC-50
01CY ATTN CODE 5404 J. GALET

COMMANDER
NAVAL OCEAN SYSTEMS CENTER
SAN DIEGO, CA 92152
03CY ATTN CODE 532 W. MOLER
01CY ATTN CODE 0230 C. BAGGETT
01CY ATTN CODE 81 R. EASTMAN

DIRECTOR
NAVAL RESEARCH LABORATORY
WASHINGTON, D.C. 20375
01CY ATTN CODE 4700 T. P. COFFE (25 CYS IF UN, 1 CY IF CLASS)
01CY ATTN CODE 4701 JACK D. BROWN
01CY ATTN CODE 4780 BRANCH HEAD (150 CYS IF UN, 1 CY IF CLASS)
01CY ATTN CODE 7500 HQ COMM DIR BRUCE WALD
01CY ATTN CODE 7550 J. DAVIS
01CY ATTN CODE 7580
01CY ATTN CODE 7551
01CY ATTN CODE 7555
01CY ATTN CODE 4730 E. MCLEAN
01CY ATTN CODE 4127 C. JOHNSON

COMMANDER
NAVAL SEA SYSTEMS COMMAND
WASHINGTON, D.C. 20362
01CY ATTN CAPT R. PITKIN

COMMANDER
NAVAL SPACE SURVEILLANCE SYSTEM
DAHLGREN, VA 22448
01CY ATTN CAPT J. H. BURTON

OFFICER-IN-CHARGE
NAVAL SURFACE WEAPONS CENTER
WHITE OAK, SILVER SPRING, MD 20910
01CY ATTN CODE F31

DIRECTOR
STRATEGIC SYSTEMS PROJECT OFFICE
DEPARTMENT OF THE NAVY
WASHINGTON, D.C. 20376
01CY ATTN NSP-2141
01CY ATTN NSSP-2722 FRED WIMBERLY

NAVAL SPACE SYSTEM ACTIVITY
P. O. BOX 92960
WORLDWAY POSTAL CENTER
LOS ANGELES, CALIF. 90009
01CY ATTN A. B. HAZZARD

COMMANDER
NAVAL SURFACE WEAPONS CENTER
DAHLGREN LABORATORY
DAHLGREN, VA 22448
01CY ATTN CODE DF-14 R. BUTLER

COMMANDING OFFICER
NAVY SPACE SYSTEMS ACTIVITY
P.O. BOX 92960
WORLDWAY POSTAL CENTER
LOS ANGELES, CA. 90009
01CY ATTN CODE 52

OFFICE OF NAVAL RESEARCH
ARLINGTON, VA 22217
01CY ATTN CODE 465
01CY ATTN CODE 461
01CY ATTN CODE 402
01CY ATTN CODE 420
01CY ATTN CODE 421

COMMANDER
AEROSPACE DEFENSE COMMAND/DC
DEPARTMENT OF THE AIR FORCE
ENT AFB, CO 80912
01CY ATTN DC MR. LONG

COMMANDER
AEROSPACE DEFENSE COMMAND/XPD
DEPARTMENT OF THE AIR FORCE
ENT AFB, CO 80912
01CY ATTN XPDQQ
01CY ATTN XP

AIR FORCE GEOPHYSICS LABORATORY
HANSCOM AFB, MA 01731
01CY ATTN OPR HAROLD GARDNER
01CY ATTN OPR-1 JAMES C. ULWICK
01CY ATTN LKB KENNETH S. W. CHAMPION
01CY ATTN OPR ALVA T. STAIR
01CY ATTN PHP JULES AARONS
01CY ATTN PHD JURGEN BUCHAU
01CY ATTN PHD JOHN P. MULLEN

AF WEAPONS LABORATORY
KIRTLAND AFB, NM 87117
01CY ATTN SUL
01CY ATTN CA ARTHUR H. GUENTHER
01CY ATTN DYC CAPT J. BARRY
01CY ATTN DYC JOHN M. KAMM
01CY ATTN DYT CAPT MARK A. FRY
01CY ATTN DES MAJ GARY GANONG
01CY ATTN DYC J. JANNI

AFTAC
PATRICK AFB, FL 32925
01CY ATTN TF/MAJ WILEY
01CY ATTN TN

AIR FORCE AVIONICS LABORATORY
WRIGHT-PATTERSON AFB, OH 45433
01CY ATTN AAD WADE HUNT
01CY ATTN AAD ALLEN JOHNSON

DEPUTY CHIEF OF STAFF
RESEARCH, DEVELOPMENT, & ACQ
DEPARTMENT OF THE AIR FORCE
WASHINGTON, D.C. 20330
01CY ATTN AFRDQ

HEADQUARTERS
ELECTRONIC SYSTEMS DIVISION/XR
DEPARTMENT OF THE AIR FORCE
HANSCOM AFB, MA 01731
01CY ATTN XR J. DEAS

HEADQUARTERS
ELECTRONIC SYSTEMS DIVISION/YSEA
DEPARTMENT OF THE AIR FORCE
HANSCOM AFB, MA 01731
01CY ATTN YSEA

HEADQUARTERS
ELECTRONIC SYSTEMS DIVISION/DC
DEPARTMENT OF THE AIR FORCE
HANSCOM AFB, MA 01731
01CY ATTN DCKC MAJ J.C. CLARK

COMMANDER
FOREIGN TECHNOLOGY DIVISION, AFSC
WRIGHT-PATTERSON AFB, OH 45433
01CY ATTN NICD LIBRARY
01CY ATTN ETDP B. BALLARD

COMMANDER
ROME AIR DEVELOPMENT CENTER, AFSC
GRIFFISS AFB, NY 13441
01CY ATTN DOC LIBRARY/TSLD
01CY ATTN OCSE V. COYNE

SAMSO/SZ
POST OFFICE BOX 92960
WORLDWAY POSTAL CENTER
LOS ANGELES, CA 90009
(SPACE DEFENSE SYSTEMS)
01CY ATTN SZJ

STRATEGIC AIR COMMAND/XPFS
OFFUTT AFB, NB 68113
01CY ATTN XPFS MAJ B. STEPHAN
01CY ATTN ADWATE MAJ BRUCE BAUER
01CY ATTN NRT
01CY ATTN DOK CHIEF SCIENTIST

SAMSO/SK
P. O. BOX 92960
WORLDWAY POSTAL CENTER
LOS ANGELES, CA 90009
01CY ATTN SKA (SPACE COMM SYSTEMS) M. CLAVIN

SAMSO/MN
NORTON AFB, CA 92409
(MINUTEMAN)
01CY ATTN MNNL LTC KENNEDY

COMMANDER
ROME AIR DEVELOPMENT CENTER, AFSC
HANSCOM AFB, MA 01731
01CY ATTN EEP A. LORENTZEN

DEPARTMENT OF ENERGY
ALBUQUERQUE OPERATIONS OFFICE
P. O. BOX 5400
ALBUQUERQUE, NM 87115
01CY ATTN DOC CON FOR D. SHERWOOD

DEPARTMENT OF ENERGY
LIBRARY ROOM G-042
WASHINGTON, D.C. 20545
01CY ATTN DOC CON FOR A. LABOWITZ

EG&G, INC.
LOS ALAMOS DIVISION
P. O. BOX 809
LOS ALAMOS, NM 85544
01CY ATTN DOC CON FOR J. BREEDLOVE

UNIVERSITY OF CALIFORNIA
LAWRENCE LIVERMORE LABORATORY
P. O. BOX 808
LIVERMORE, CA 94550
01CY ATTN DOC CON FOR TECH INFO DEPT
01CY ATTN DOC CON FOR L-389 R. OTT
01CY ATTN DOC CON FOR L-31 R. HAGER
01CY ATTN DOC CON FOR L-46 F. SEWARD

LOS ALAMOS SCIENTIFIC LABORATORY
P. O. BOX 1663
LOS ALAMOS, NM 87545
01CY ATTN DOC CON FOR J. WOLCOTT
01CY ATTN DOC CON FOR R. F. TASCHEK
01CY ATTN DOC CON FOR E. JONES
01CY ATTN DOC CON FOR J. MALIK
01CY ATTN DOC CON FOR R. JEFFRIES
01CY ATTN DOC CON FOR J. ZINN
01CY ATTN DOC CON FOR P. KEATON
01CY ATTN DOC CON FOR D. WESTERVELT

SANDIA LABORATORIES
P. O. BOX 5800
ALBUQUERQUE, NM 87115
01CY ATTN DOC CON FOR J. MARTIN
01CY ATTN DOC CON FOR W. BROWN
01CY ATTN DOC CON FOR A. THORNBROUGH
01CY ATTN DOC CON FOR T. WRIGHT
01CY ATTN DOC CON FOR D. DAHLGREN
01CY ATTN DOC CON FOR 3141
01CY ATTN DOC CON FOR SPACE PROJECT DIV

SANDIA LABORATORIES
LIVERMORE LABORATORY
P. O. BOX 969
LIVERMORE, CA 94550
01CY ATTN DOC CON FOR B. MURPHEY
01CY ATTN DOC CON FOR T. COOK

OFFICE OF MILITARY APPLICATION
DEPARTMENT OF ENERGY
WASHINGTON, D.C. 20545
01CY ATTN DOC CON FOR D. GALE

OTHER GOVERNMENT

CENTRAL INTELLIGENCE AGENCY
ATTN RD/SI, RM 5G48, HQ BLDG
WASHINGTON, D.C. 20505
01CY ATTN OSI/PSID RM 5F 19

DEPARTMENT OF COMMERCE
NATIONAL BUREAU OF STANDARDS
WASHINGTON, D.C. 20234
(ALL CORRES: ATTN SEC OFFICER FOR)
01CY ATTN R. MOORE

INSTITUTE FOR TELECOM SCIENCES
NATIONAL TELECOMMUNICATIONS & INFO ADMIN
BOULDER, CO 80303
01CY ATTN A. JEAN (UNCLASS ONLY)
01CY ATTN W. UTLAUT
01CY ATTN D. CROMBIE
01CY ATTN L. BERRY

NATIONAL OCEANIC & ATMOSPHERIC ADMIN
ENVIRONMENTAL RESEARCH LABORATORIES
DEPARTMENT OF COMMERCE
BOULDER, CO 80302
01CY ATTN R. GRUBB
01CY ATTN AERONOMY LAB G. REID

DEPARTMENT OF DEFENSE CONTRACTORS

AEROSPACE CORPORATION
P. O. BOX 92957
LOS ANGELES, CA 90009
01CY ATTN I. GARFUNKEL
01CY ATTN T. SALMI
01CY ATTN V. JOSEPHSON
01CY ATTN S. BOWER
01CY ATTN N. STOCKWELL
01CY ATTN D. OLSEN
01CY ATTN J. CARTER
01CY ATTN F. MORSE
01CY ATTN SMFA FOR PWW

ANALYTICAL SYSTEMS ENGINEERING CORP
5 OLD CONCORD ROAD
BURLINGTON, MA 01803
01CY ATTN RADIO SCIENCES

BERKELEY RESEARCH ASSOCIATES, INC.
P. O. BOX 983
BERKELEY, CA 94701
01CY ATTN J. WORKMAN

BOEING COMPANY, THE
P. O. BOX 3707
SEATTLE, WA 98124
01CY ATTN G. KEISTER
01CY ATTN D. MURRAY
01CY ATTN G. HALL
01CY ATTN J. KENNEY

CALIFORNIA AT SAN DIEGO, UNIV OF
IPAPS, B-019
LA JOLLA, CA 92093
01CY ATTN HENRY G. BOOKER

BROWN ENGINEERING COMPANY, INC.
CUMMINGS RESEARCH PARK
HUNTSVILLE, AL 35807
01CY ATTN ROMEO A. DELIBERIS

CHARLES STARK DRAPER LABORATORY, INC.
555 TECHNOLOGY SQUARE
CAMBRIDGE, MA 02139
01CY ATTN D. B. COX
01CY ATTN J. P. GILMORE

COMPUTER SCIENCES CORPORATION
6565 ARLINGTON BLVD
FALLS CHURCH, VA 22046
01CY ATTN H. BLANK
01CY ATTN JOHN SPOOR
01CY ATTN C. NAIL

COMSAT LABORATORIES
LINTHICUM ROAD
CLARKSBURG, MD 20734
01CY ATTN G. HYDE

CORNELL UNIVERSITY
DEPARTMENT OF ELECTRICAL ENGINEERING
ITHACA, NY 14850
01CY ATTN D. T. FARLEY JR

ELECTROSPACE SYSTEMS, INC.
BOX 1359
RICHARDSON, TX 75080
01CY ATTN H. LOGSTON
01CY ATTN SECURITY (PAUL PHILLIPS)

ESL INC.
495 JAVA DRIVE
SUNNYVALE, CA 94086
01CY ATTN J. ROBERTS
01CY ATTN JAMES MARSHALL
01CY ATTN C. W. PRETTIE

FORD AEROSPACE & COMMUNICATIONS CORP
3939 FABIAN WAY
PALO ALTO, CA 94303
01CY ATTN J. T. MATTINGLEY

GENERAL ELECTRIC COMPANY
SPACE DIVISION
VALLEY FORGE SPACE CENTER
GODDARD BLVD KING OF PRUSSIA
P. O. BOX 8555
PHILADELPHIA, PA 19101
01CY ATTN M. H. BORTNER SPACE SCI LAB

GENERAL ELECTRIC COMPANY
P. O. BOX 1122
SYRACUSE, NY 13201
01CY ATTN F. REIBERT

GENERAL ELECTRIC COMPANY
TEMPO-CENTER FOR ADVANCED STUDIES
816 STATE STREET (P.O. DRAWER QQ)
SANTA BARBARA, CA 93102
01CY ATTN DASIAC
01CY ATTN DON CHANDLER
01CY ATTN TOM BARRETT
01CY ATTN TIM STEPHANS
01CY ATTN WARREN S. KNAPP
01CY ATTN WILLIAM MCNAMARA
01CY ATTN B. GAMBILL
01CY ATTN MACK STANTON

GENERAL ELECTRIC TECH SERVICES CO., INC.
HMES
COURT STREET
SYRACUSE, NY 13201
01CY ATTN G. MILLMAN

GENERAL RESEARCH CORPORATION
SANTA BARBARA DIVISION
P. O. BOX 6770
SANTA BARBARA, CA 93111
01CY ATTN JOHN ISE JR
01CY ATTN JOEL GARBARINO

GEOPHYSICAL INSTITUTE
UNIVERSITY OF ALASKA
FAIRBANKS, AK 99701
(ALL CLASS ATTN: SECURITY OFFICER)
01CY ATTN T. N. DAVIS (UNCL ONLY)
01CY ATTN NEAL BROWN (UNCL ONLY)
01CY ATTN TECHNICAL LIBRARY

GTE SYLVANIA, INC.
ELECTRONICS SYSTEMS GRP-EASTERN DIV
77 A STREET
NEEDHAM, MA 02194
01CY ATTN MARSHAL CROSS

ILLINOIS, UNIVERSITY OF
DEPARTMENT OF ELECTRICAL ENGINEERING
URBANA, IL 61803
01CY ATTN K. YEH

ILLINOIS, UNIVERSITY OF
107 COBLE HALL
801 S. WRIGHT STREET
URBANA, IL 60680
(ALL CORRES ATTN SECURITY SUPERVISOR FOR)
01CY ATTN K. YEH

INSTITUTE FOR DEFENSE ANALYSES
400 ARMY-NAVY DRIVE
ARLINGTON, VA 22202
01CY ATTN J. M. AEIN
01CY ATTN ERNEST BAUER
01CY ATTN HANS WOLFHARD
01CY ATTN JOEL BENGSTON

HSS, INC.
2 ALFRED CIRCLE
BEDFORD, MA 01730
01CY ATTN DONALD HANSEN

INTL TEL & TELEGRAPH CORPORATION
500 WASHINGTON AVENUE
NUTLEY, NJ 07110
01CY ATTN TECHNICAL LIBRARY

JAYCOR
1401 CAMINO DEL MAR
DEL MAR, CA 92014
01CY ATTN S. R. GOLDMAN

JOHNS HOPKINS UNIVERSITY
APPLIED PHYSICS LABORATORY
JOHNS HOPKINS ROAD
LAUREL, MD 20810
01CY ATTN DOCUMENT LIBRARIAN
01CY ATTN THOMAS POTEMRA
01CY ATTN JOHN DASSOULAS

LOCKHEED MISSILES & SPACE CO INC
P. O. BOX 504
SUNNYVALE, CA 94088
01CY ATTN DEPT 60-12
01CY ATTN D. R. CHURCHILL

LOCKHEED MISSILES AND SPACE CO INC
3251 HANOVER STREET
PALO ALTO, CA 94304
01CY ATTN MARTIN WALT DEPT 52-10
01CY ATTN RICHARD G. JOHNSON DEPT 52-12
01CY ATTN W. L. IMHOF DEPT 52-12

KAMAN SCIENCES CORP
P. O. BOX 7463
COLORADO SPRINGS, CO 80933
01CY ATTN T. MEAGHER

LINKABIT CORP
10453 ROSELLE
SAN DIEGO, CA 92121
01CY ATTN IRWIN JACOBS

M.I.T. LINCOLN LABORATORY
P. O. BOX 73
LEXINGTON, MA 02173
01CY ATTN DAVID M. TOWLE
01CY ATTN P. WALDRON
01CY ATTN L. LOUGHLIN
01CY ATTN D. CLARK

MARTIN MARIETTA CORP
ORLANDO DIVISION
P. O. BOX 5837
ORLANDO, FL 32805
01CY ATTN R. HEFFNER

MCDONNELL DOUGLAS CORPORATION
5301 BOLSA AVENUE
HUNTINGTON BEACH, CA 92647
01CY ATTN N. HARRIS
01CY ATTN J. MOULE
01CY ATTN GEORGE MROZ
01CY ATTN W. OLSON
01CY ATTN R. W. HALPRIN
01CY ATTN TECHNICAL LIBRARY SERVICES

MISSION RESEARCH CORPORATION
735 STATE STREET
SANTA BARBARA, CA 93101
01CY ATTN P. FISCHER
01CY ATTN W. F. CREVIER
01CY ATTN STEVEN L. GUTSCHE
01CY ATTN D. SAPPENFIELD
01CY ATTN R. BOGUSCH
01CY ATTN R. HENDRICK
01CY ATTN RALPH KILB
01CY ATTN DAVE SOWLE
01CY ATTN F. FAJEN
01CY ATTN M. SCHEIBE
01CY ATTN CONRAD L. LONGMIRE
01CY ATTN WARREN A. SCHLUETER

MITRE CORPORATION, THE
P. O. BOX 208
BEDFORD, MA 01730
01CY ATTN JOHN MORGANSTERN
01CY ATTN G. HARDING
01CY ATTN C. E. CALLAHAN

MITRE CORP
WESTGATE RESEARCH PARK
1820 DOLLY MADISON BLVD
MCLEAN, VA 22101
01CY ATTN W. HALL
01CY ATTN W. FOSTER

PACIFIC-SIERRA RESEARCH CORP
1456 CLOVERFIELD BLVD.
SANTA MONICA, CA 90404
01CY ATTN E. C. FIELD JR

PENNSYLVANIA STATE UNIVERSITY
IONOSPHERE RESEARCH LAB
318 ELECTRICAL ENGINEERING EAST
UNIVERSITY PARK, PA 16802
(NO CLASSIFIED TO THIS ADDRESS)
01CY ATTN IONOSPHERIC RESEARCH LAB

PHOTOMETRICS, INC.
442 MARRETT ROAD
LEXINGTON, MA 02173
01CY ATTN IRVING L. KOFSKY

PHYSICAL DYNAMICS INC.
P. O. BOX 3027
BELLEVUE, WA 98009
01CY ATTN E. J. FREMOUW

PHYSICAL DYNAMICS INC.
P. O. BOX 10367
OAKLAND, CA. 94610
ATTN: A. THOMSON

R & D ASSOCIATES
P. O. BOX 9695
MARINA DEL REY, CA 90291
01CY ATTN FORREST GILMORE
01CY ATTN BRYAN GABBARD
01CY ATTN WILLIAM B. WRIGHT JR
01CY ATTN ROBERT F. LELEVIER
01CY ATTN WILLIAM J. KARZAS
01CY ATTN H. ORY
01CY ATTN C. MACDONALD
01CY ATTN R. TURCO

RAND CORPORATION, THE
1700 MAIN STREET
SANTA MONICA, CA 90406
01CY ATTN CULLEN CRAIN
01CY ATTN ED BEDROZIAN

RIVERSIDE RESEARCH INSTITUTE
80 WEST END AVENUE
NEW YORK, NY 10023
01CY ATTN VINCE TRAPANI

SCIENCE APPLICATIONS, INC.
P. O. BOX 2351
LA JOLLA, CA 92038
01CY ATTN LEWIS M. LINSON
01CY ATTN DANIEL A. HAMLIN
01CY ATTN D. SACHS
01CY ATTN E. A. STRAKER
01CY ATTN CURTIS A. SMITH
01CY ATTN JACK MCDOUGALL

RAYTHEON CO.
528 BOSTON POST ROAD
SUDBURY, MA 01776
01CY ATTN BARBARA ADAMS

Science Applications, Inc.
1700 Goodridge Dr.
McLean, Va. 22102
01 cy ATTN J. COCKAYNE

Lockheed Missile & Space Co., Inc.
Huntsville Research & Engineering Center
4800 Bradford Dr.
Huntsville, Ala. 35807
01 cy ATTN DALE H. DIVIS

SRI INTERNATIONAL
333 RAVENSWOOD AVENUE
MENLO PARK, CA 94025
01CY ATTN DONALD NEILSON
01CY ATTN ALAN BURNS
01CY ATTN G. SMITH
01CY ATTN L. L. COBB
01CY ATTN DAVID A. JOHNSON
01CY ATTN WALTER G. CHESNUT
01CY ATTN CHARLES L. RINO
01CY ATTN WALTER JAYE
01CY ATTN M. BARON
01CY ATTN RAY L. LEADABRAND
01CY ATTN G. CARPENTER
01CY ATTN G. PRICE
01CY ATTN J. PETERSON
01CY ATTN R. HAKE, JR.
01CY ATTN V. GONZALES
01CY ATTN D. MCDANIEL

TECHNOLOGY INTERNATIONAL CORP
75 WIGGINS AVENUE
BEDFORD, MA 01730
01CY ATTN W. P. BOQUIST

TRW DEFENSE & SPACE SYS GROUP
ONE SPACE PARK
REDONDO BEACH, CA 90278
01CY ATTN R. K. PLEBUCH
01CY ATTN S. ALTSCHULER
01CY ATTN D. DEE

VISIDYNE, INC.
19 THIRD AVENUE
NORTH WEST INDUSTRIAL PARK
BURLINGTON, MA 01803
01CY ATTN CHARLES HUMPHREY
01CY ATTN J. W. CARPENTER

IONOSPHERIC MODELING DISTRIBUTION LIST
UNCLASSIFIED ONLY

PLEASE DISTRIBUTE ONE COPY TO EACH OF THE FOLLOWING PEOPLE:

ADVANCED RESEARCH PROJECTS AGENCY (ARPA)
STRATEGIC TECHNOLOGY OFFICE
ARLINGTON, VIRGINIA

CAPT. DONALD M. LEVINE

NAVAL RESEARCH LABORATORY
WASHINGTON, D.C. 20375

DR. P. MANGE
DR. R. MEIER
DR. E. SZUSZCZEWICZ - CODE 4127

DR. J. GOODMAN - CODE 7560

SCIENCE APPLICATIONS, INC.
1250 PROSPECT PLAZA
LA JOLLA, CALIFORNIA 92037

DR. D. A. HAMLIN
DR. L. LINSON
DR. D. SACHS

DIRECTOR OF SPACE AND ENVIRONMENTAL LABORATORY
NOAA
BOULDER, COLORADO 80302

DR. A. GLENN JEAN
DR. G. W. ADAMS
DR. D. N. ANDERSON
DR. K. DAVIES
DR. R. F. DONNELLY

A. F. GEOPHYSICS LABORATORY
L. G. HANSOM FIELD
BEDFORD, MASS. 01730

DR. T. ELKINS
DR. W. SWIDER
MRS. R. SAGALYN
DR. J. M. FORBES
DR. T. J. KENESHEA
DR. J. AARONS

OFFICE OF NAVAL RESEARCH
800 NORTH QUINCY STREET
ARLINGTON, VIRGINIA 22217

DR. H. MULLANEY

COMMANDER
NAVAL ELECTRONICS LABORATORY CENTER
SAN DIEGO, CALIFORNIA 92152

DR. M. BLEIWEISS
DR. I. ROTHMULLER
DR. V. HILDEBRAND
MR. R. ROSE

U. S. ARMY ABERDEEN RESEARCH AND DEVELOPMENT CENTER
BALLISTIC RESEARCH LABORATORY
ABERDEEN, MARYLAND

DR. J. HEIMERL

COMMANDER
NAVAL AIR SYSTEMS COMMAND
DEPARTMENT OF THE NAVY
WASHINGTON, D.C. 20360

DR. T. CZUBA

HARVARD UNIVERSITY
HARVARD SQUARE
CAMBRIDGE, MASS. 02138

DR. M. B. MCELROY
DR. R. LINDZEN

PENNSYLVANIA STATE UNIVERSITY
UNIVERSITY PARK, PENNSYLVANIA 16802

DR. J. S. NISBET
DR. P. R. ROHRBAUGH
DR. D. E. BARAN
DR. L. A. CARPENTER
DR. M. LEE
DR. R. DIVANY
DR. P. BENNETT
DR. E. KLEVANS

UNIVERSITY OF CALIFORNIA, LOS ANGELES
405 HILLGARD AVENUE
LOS ANGELES, CALIFORNIA 90024

DR. F. V. CORONITI
DR. C. KENNEL

UNIVERSITY OF CALIFORNIA, BERKELEY
BERKELEY, CALIFORNIA 94720

DR. M. HUDSON

UTAH STATE UNIVERSITY
4TH N. AND 8TH STREETS
LOGAN, UTAH 84322

DR. P. M. BANKS
DR. R. HARRIS
DR. V. PETERSON
DR. R. MEGILL
DR. K. BAKER

CORNELL UNIVERSITY
ITHACA, NEW YORK 14850

DR. W. E. SWARTZ
DR. R. SUDAN
DR. D. FARLEY
DR. M. KELLEY

NASA
GODDARD SPACE FLIGHT CENTER
GREENBELT, MARYLAND 20771

DR. S. CHANDRA
DR. K. MAEDO

PRINCETON UNIVERSITY
PLASMA PHYSICS LABORATORY
PRINCETON, NEW JERSEY 08540

DR. F. PERKINS
DR. E. FRIEMAN

INSTITUTE FOR DEFENSE ANALYSIS
400 ARMY/NAVY DRIVE
ARLINGTON, VIRGINIA 22202

DR. E. BAUER

UNIVERSITY OF MARYLAND
COLLEGE PARK, MD 20742
DR. K. PAPADOPOULOS
DR. E. OTT

UNIVERSITY OF PITTSBURGH
PITTSBURGH, PA. 15213

DR. N. ZABUSKY
DR. M. BIONDI

UNIVERSITY OF CALIFORNIA
LOS ALAMOS SCIENTIFIC LABORATORY
J-10, MS-664
LOS ALAMOS, NEW MEXICO 87545

M. PONGRATZ
D. SIMONS
G. BARASCH
L. DUNCAN

DAT
FILM